How to cite: *Angew. Chem. Int. Ed.* **2024**, *63*, e202401706
doi.org/10.1002/anie.202401706

Porous Organic Materials | Hot Paper

A Novel Homoconjugated Propellane Triimide: Synthesis, Structural Analyses, and Gas Separation

Yan Chen[+], Yongting Zhao[+], Yubo Zhao[+], Xiangping Chen, Xinyue Liu, Lin Li, Dapeng Cao, Shitao Wang,* and Lei Zhang**

Abstract: Rigid three-dimensional (3D) polycyclic propellanes have garnered interest due to their unique conformational spaces, which display great potential use in selectivity, separation and as models to study through-space electronic interactions. Herein we report the synthesis of a novel rigid propellane, trinaphtho-[3.3.3]propellane triimide, which comprises three imide groups embedded on a trinaphtho[3.3.3]propellane. This propellane triimide exhibits large bathochromic shift, amplified molar absorptivity, enhanced fluorescence, and lower reduction potential when compared to the subunits. Computational and experimental studies reveal that the effective through-space π-orbitals interacting (homoconjugation) occurs between the subunits. Single-crystal XRD analysis reveals that the propellane triimide has a highly quasi-D_{3h} symmetric skeleton and readily crystallizes into different superstructures by changing alkyl chains at the imide positions. In particular, the porous 3D superstructure with S-shaped channels is promising for taking up ethane (C_2H_6) with very good selectivity over ethylene (C_2H_4), which can purify C_2H_4 from C_2H_6/C_2H_4 in a single separation step. This work showcases a new class of rare 3D polycyclic propellane with intriguing electronic and supramolecular properties.

The rigid three-dimensional (3D) polycyclic compounds containing aromatic rings which are typically fused on [2.2.2]bicyclic and [3.3.3.0]tricyclic ring systems, often referred as iptycene and propellane, have aroused continuous interest not only due to as synthetic targets in their own right, but also as building blocks in construction of supramolecular systems with new properties.[1] In particular, the intramolecular free volumes in the systems afford the opportunity for binding to suitably sized species, which can be used in sensory responses, molecular recognition, and gas separation.[2] In addition, these systems are being extensively explored for use in molecular electronics and nanotechnology.[3] One of the classic 3D polycyclic compounds is triptycene, and its chemistry has been considerably developed during the past decades.[4] Functionalization at the peripheral positions of the benzene rings offers great potential for creating a variety of triptycene derivatives that bear several functional groups fixed in well-defined spatial orientation within the molecule.[5] However, the development of strategies for construction of new 3D scaffolds present significant synthetic challenges, as a consequence, the structure diversity is still low, particularly with respect to control over the homoconjugation effect, which has a profound impact on molecular properties.[6]

Herein we report the synthesis and characterization of a novel rigid quasi-D_{3h} symmetric polycyclic propellane, trinaphtho[3.3.3]propellane triimide, which comprises three imide groups embedded on a trinaphtho[3.3.3]propellane. As with triptycene, trinaphtho[3.3.3]propellane is a rigid quasi-D_{3h} symmetric molecule, in which the three nathphalene subunits are cofacially oriented at an angle of ~120°.[7] It has been demonstrated that the nathphalene subunit on the propellane is likely to confer electronic interactions via through space, which makes the system ideal for studying the homoconjugation effect.[8] From a structural point of view, this propellane triimide can be viewed as three nathphalene monoimides (NMI) fused on a [3.3.3]propellane. Due to its electron-deficient nature and unique redox properties, NMI represents a highly versatile building block for the construction of unusual polycyclic nanostructures.[9] For example, Wudl et al. reported the synthesis of a planar decacyclene triimide, in which three NMI units are fused on a benzene ring, serving as electron acceptor for organic solar cells (Figure 1).[10] Recently, Stępień et al. successfully synthesized a saddle-shaped nanocarbon comprising a quadruply NMI-fused derivative of 1,3,5,7-cyclooctatetraene, which allows to accept up to eight electrons (Figure 1).[11] These works demonstrate the scaffold leads to key differences in electronic structures, strongly influencing optoelectronic and supramolecular properties, which encourage us to pursue the synthesis of a new type of

[*] Dr. Y. Chen,[+] Y. Zhao,[+] Y. Zhao,[+] X. Chen, X. Liu, Prof. D. Cao, Prof. S. Wang, Prof. L. Zhang
Beijing Advanced Innovation Center for Soft Matter Science and Engineering, State Key Lab of Organic-Inorganic Composites, College of Materials Science and Engineering
Beijing University of Chemical Technology
100029 Beijing (P. R. China)
E-mail: zhl@mail.buct.edu.cn
stwang@buct.edu.cn

Dr. L. Li
School of Materials Science and Engineering, National Institute for Advanced Materials, TKL of Metal and Molecule-Based Material Chemistry
Nankai University
300350 Tianjin (P. R. China)
E-mail: lilin@nankai.edu.cn

[+] These authors contributed equally to this work.

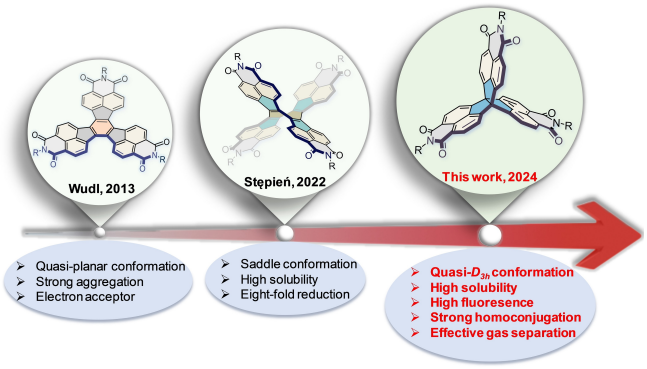

Figure 1. Polycyclic hydrocarbons with multiple imides: structural evolution from quasi-planar to quasi-D_{3h} conformations.

propellane solely composed of NMI units. The resulting trinaphtho[3.3.3] propellane triimide exhibits a highly quasi-D_{3h} symmetric skeleton with strong homoconjugation. Notably, compared with triperyleno[3.3.3]propellane triimide,[8c] in which the through-space electronic communication among the three perylenemonoimide units is relatively weak, trinaphtho[3.3.3]propellane triimide exhibits significantly enhanced through-space electron sharing, which should have a profound impact on electronic and supramolecular properties.

Our synthesis was initiated by the bromination of trinaphtho[3.3.3]propellane, which produced brominated trinaphtho[3.3.3]propellane **1**[7c] as a mixture of regioisomers (*3,10,15*-tribromo trinaphtho[3.3.3]propellane and *3,10,16*-tribromo trinaphtho[3.3.3]propellane) in a high yield (Scheme 1). Then, a Pd-catalyzed decarboxylative coupling[12] of potassium 2-ethoxy-2-oxoacetate with **1** produced trinaphtho[3.3.3]propellane triester **2** in 80 % yield, which was subjected to a Pd-catalyzed regioselective *ortho*-bromination reaction[13] in the present of $Pd(OAc)_2$ with $Na_2S_2O_8$ as the oxidant, affording **3** in 60 % yield. Next, the Pd-catalyzed carbonylation[14] of **3** with a highly reactive 2,4,6-trichlorophenyl formate in the present of $Pd(OAc)_2$ and xantphos provided hexaester **4** in 80 % yield. Hydrolyzation of **4** under the present of KOH led to hexacarboxylic acid **5**, followed by a cyclization reaction in acetic anhydride to give trianhydride **6**. With the trianhydride in hand, direct imidization of **6** with *n*-octylamine and *2,2,3,3,4,4,4*-heptafluorobutylamine in *N,N*-dimethylformamide (DMF) provided the desired trinaphtho[3.3.3]propellane triimides **7a** and **7b** in 50 % yield, respectively, which are soluble in common solvents, such as dichloromethane, chloroform, tetrahydrofuran, and toluene.

As shown in Figure 2a, the absorption maxima of **7a** and **7b** at 385 nm is red-shifted by 35 nm relative to their corresponding subunits (C_8H_{17}-NMI and C_3F_7-NMI) that occur at 350 nm, indicating the effective homoconjugation among the subunits. This homoconjugation effect is also reflected in the amplification of absorption coefficiencies of **7a** and **7b** (45000 M^{-1} cm^{-1}), which are significantly larger than that of the sum of the three subunits (3×12000 M^{-1} cm^{-1}) (Table S2). Time dependent density functional theory (TD-DFT) calculations at the B3LYP/6-31G(d) level of theory predict the low-energy absorbance corresponds to the highest occupied molecular orbital (HOMO) to the lowest unoccupied molecular orbital (LUMO) transition (λ_{calc} = 398 nm, f = 0.283) (Figure S4 and Table S3), which matches well to the observed spectrum. Remarkably, in comparing C_8H_{17}-NMI and C_3F_7-NMI to **7a** and **7b**, the significant increase in emission quantum yields with longer lifetimes are observed (Table S2), which are likely due to the rigidity of the 3D scaffold that might reduce the vibrational relaxation pathways and suppress fluorescence self-quenching.

Cyclic voltammetry (CV) and differential pulse voltammetry (DPV) studies were performed in dichloromethane with tetrabutylammonium hexafluorophosphate as the supporting electrolyte, and the reduction potentials are determined relative to ferrocene/ferrocenium (Fc/Fc^+), assuming an ionization energy of 4.8 eV for ferrocene[15] (Figure 2b and Table S2). In contrast to the CVs of C_8H_{17}-NMI and C_3F_7-NMI exhibiting one reversible one-electron reduction wave, the CVs of **7a** and **7b** display three reversible one-

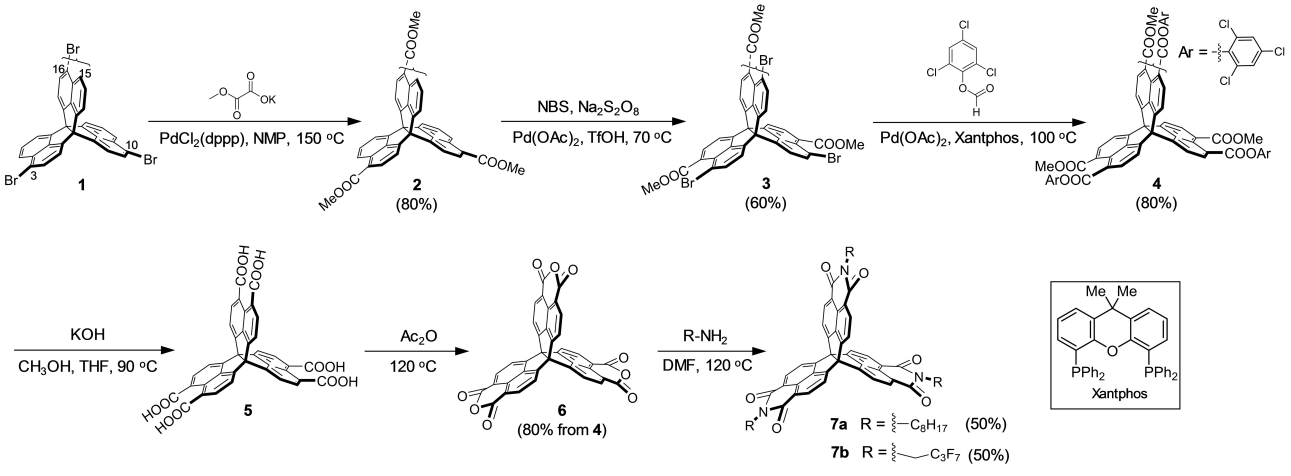

Scheme 1. Synthetic Steps to trinaphtho[3.3.3]propellane triimides. NMP = *N*-methylpyrrolidone.

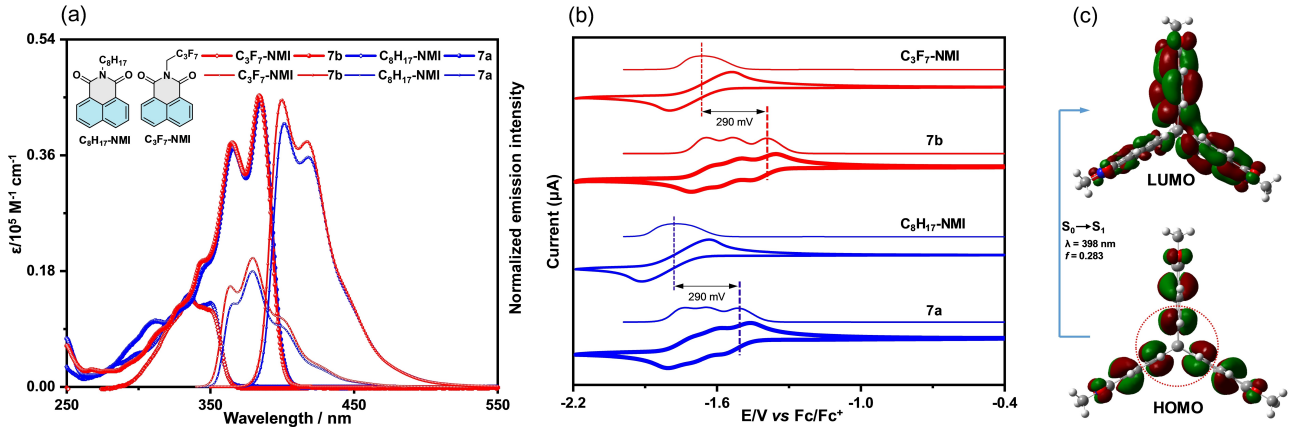

Figure 2. (a) UV/Vis absorption (thick dotted line) and fluorescence spectra (thin dotted line) of **7a**, **7b**, C_8H_{17}-NMI, and C_3F_7-NMI in chloroform (~10^{-5} M). (b) Cyclic voltammograms (thick solid line) and differential pulse voltammograms (thin solid line) of **7a**, **7b**, C_8H_{17}-NMI, and C_3F_7-NMI. (c) Molecular orbitals of trinaphtho[3.3.3]propellane triimide calculated by DFT at the B3LYP/6-31G(d) level of theory. The dashed red circle denotes the regions of electronic coupling among the NMI subunits.

electron reduction waves, indicating the imide units in **7a** and **7b** are located in close enough proximity to each other to impose repulsive Coulombic interactions that come into play when a second electron is introduced into the molecule. The first half-wave reduction potentials (E_{red}^1) of −1.48 V for **7a** and −1.36 V for **7b** are significantly shifted toward more positive by 0.29 V compared to C_8H_{17}-NMI and C_3F_7-NMI, respectively, which suggests that there is significant conjugative interactions between the subunits in **7a** and **7b**. Density functional theory (DFT) calculations at the B3LYP/6-31G(d) level of theory reveal that the HOMO is delocalized across all three subunits, while the LUMO and LUMO+1 are degenerate and delocalized over two of the three NMI subunits (Figure 2c). A clear overlapping between the LUMO orbitals around the subunits is observed, which likely results in the lowering of the LUMO level (Figure 2c). DFT calculations further identify that the favorable nodal arrangement of HOMO leads to appreciable orbital overlap between the subunits through σ-bonds of the bridgehead sp^3 carbons, which provides the electronic coupling of 134 mV according to the prediction method reported by Rathore.[6d]

Single crystals of **7a** and **7b** suitable for X-ray diffraction analysis were grown by slow diffusion of methanol into chloroform solution.[16] The X-ray crystal analysis reveals that the propellane triimide skeleton adopts a quasi-D_{3h} symmetric conformation with the dihedral angle of ~120° between the individual NMI subunits (Figures 3a and 3c). The central C–C bond (1.640 Å) of the bridgehead carbons is slightly elongated compared to the C–C bonds (1.588 Å) between two tertiary carbons.[17] The surrounding C–C bond lengths are in the range of 1.510–1.533 Å, which are close to that of the typical sp^3–sp^3 bond length (1.530 Å).

In an individual layer of **7a**, the two NMI subunits of adjacent molecules adopt a π-stacked dimer motif with a π–π distance of 3.3 Å and multiple C–H···π contacts. The adjacent π-stacks are "stitched together" along the *b*-axis to form infinite arrays with the alkyl chains interdigitated, thus, making the crystal interesting with two-dimensional (2D) character (Figure 3b). However, for compound **7b**, each NMI subunit makes somewhat limited contacts between the NMI subunit of the neighboring molecule by C···C, C···O, C–H···O contacts. Notably, the fluorine atoms are involved

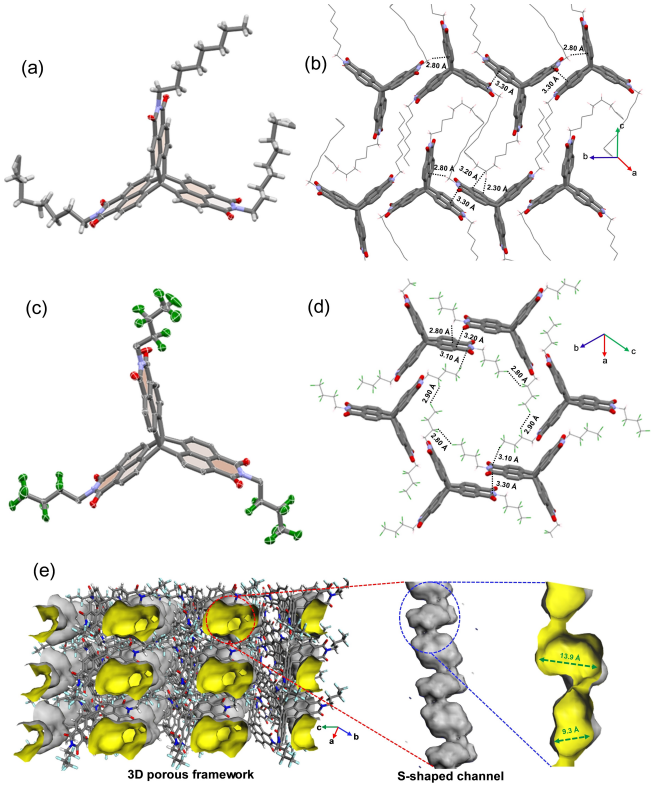

Figure 3. Crystal structures of **7a** (a) and **7b** (c); Crystal packing of **7a** (b) and **7b** (d) with the selected close contacts. (Partial hydrogen atoms are omitted for clarity); (e) 3D packing diagram and S-shaped channel of **7b**, with the void space visualized by yellow/gray (inner/outer) curved planes generated with a probe of 1.4 Å. The whole process is determined by single-crystal X-ray diffraction (SCXRD).

in multiple close F···F and F···C contacts with neighboring molecules, forming the layer with a quasi-hexagonal packing motif (Figure 3d). These layers are stacked in a slipping fashion via interlayer F···F, C–H···π, C···C contacts to form a porous 3D network with S-shaped channels (Figure 3e). Two distinct void spaces are present in the porous network, with the pore sizes of 13.9 Å and 9.3 Å, respectively.

We next investigate the porous nature of **7b**. The adsorption-desorption isotherm of nitrogen at 77 K is depicted in Figure 4a. The adsorption profile of **7b** demonstrates a pronounced elevation when P/P_0 exceeds 0.46, indicative of a "gate-opening" phenomenon,[18] which was further confirmed by in situ powder X-ray diffraction at 77 K (Figure S9). Notably, during the desorption phase, a considerable hysteresis loop manifests, reminiscent of the characteristics observed in flexible porous materials.[19] Thus, the intrinsic porosity and flexible framework in **7b** encourage us to further explore its capacity for ethane (C_2H_6)/ethylene (C_2H_4) separation, a crucial and challenging process in the petrochemical industry.[20] The single-component adsorption experiments were conducted on C_2H_6 and C_2H_4 at different temperatures (273 K, 298 K and 308 K) by using activated **7b** (Figure S10). As depicted in Figure 4b and Figure S6, the adsorption of C_2H_6 across the entire pressure range at different temperatures consistently exceeds that of C_2H_4, thereby signifying a discernible separation capability of **7b** (Table S4). At 298 K and 1 bar, the adsorbed amount of C_2H_6 for **7b** could reach approximately 17.2 $cm^3 g^{-1}$, higher than that of C_2H_4 (11.1 $cm^3 g^{-1}$). The isosteric heats of adsorption (Q_{st}) of C_2H_6 is calculated to be 28.9–40.3 kJ mol^{-1}, by using the Virial equation (Figure S8 and Table S6), which is higher than that of C_2H_4 (26.6–30.2 kJ mol^{-1}), revealing that **7b** has stronger gas bonding affinity towards C_2H_6 (Figure 4c). These results are also validated by dispersion-corrected density-functional theory calculations (DFT-D), which reveal the corresponding calculated static binding energies (ΔE, $\Delta E = E_{7b+gas} - E_{7b} - E_{gas}$) for C_2H_6 and C_2H_4 are around −24.56 and −18.05 kJ mol^{-1}, respectively. The elevated binding energy primarily emanates from the superior steric complementarity between the C_2H_6 molecule and the cavity of **7b** when juxtaposed with the C_2H_4 molecule,[21] likely due to more efficient C–H···π bonds and hydrogen bonds for C_2H_6 (Figure 5a) than those for C_2H_4 (Figure 5b). This result also leads us to conclude that the C–H···N hydrogen bonding might play a dominant role in C_2H_6-selectivity. Thus, the C_2H_6 molecules are assumed to be preferentially located in the cavity self-assembled from **7b** in neighboring layers. In addition, the corresponding selectivity of **7b** towards C_2H_6 and C_2H_4 at 1 bar is estimated to be 2.24 by the ideal solution theory (IAST, Figure 4d). This value is very close to the maximal selectivity reported for ZJU-HOF-1 (2.25),[21] surpassing those reported for other high-performance C_2H_6-selective organic adsorbents[21,22] at 298 K and 1 bar (Figure 4e and Table S5). We note that the selectivity towards C_2H_6 could simplify the C_2H_4 purification process in

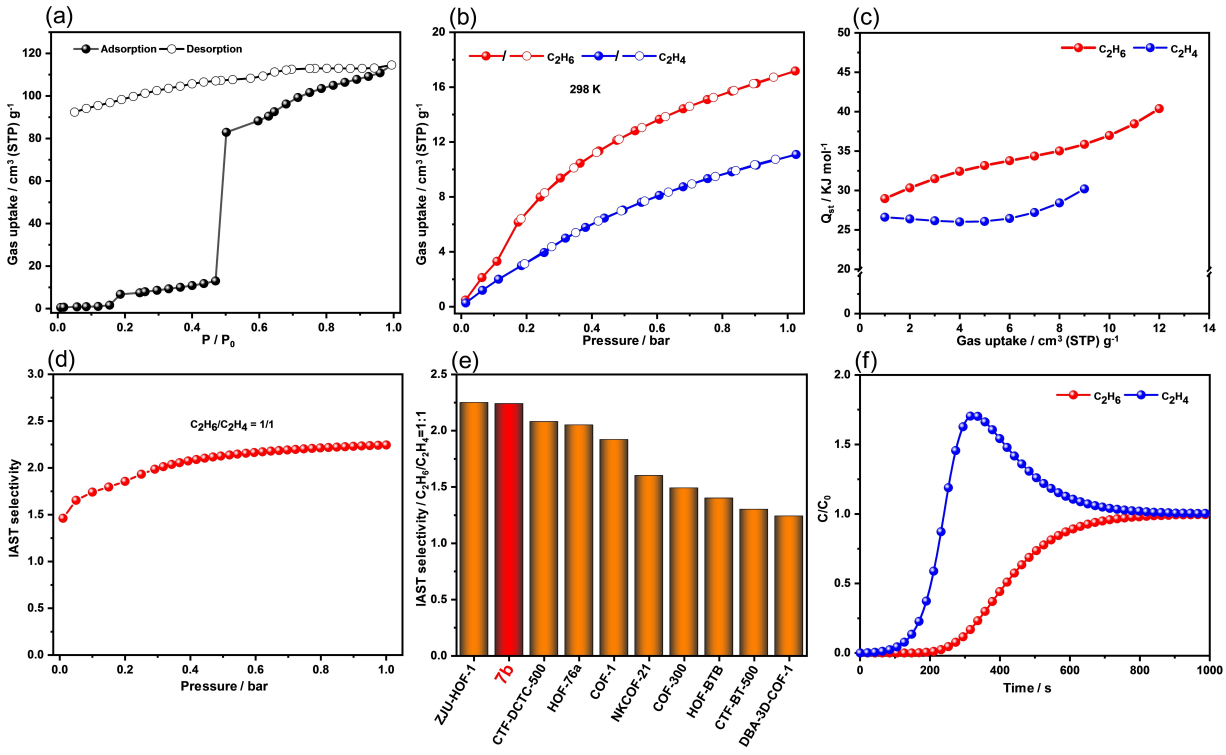

Figure 4. (a) N_2 adsorption-desorption Isotherm curves of **7b** at 77 K. (b) Single component adsorption isotherms of ethane and ethylene at 298 K. (c) Q_{st} curves for **7b**. (d) IAST selectivity of C_2H_6/C_2H_4 (1 : 1, v/v, without gas carrier) mixtures at 298 K. (e) Comparison of IAST selectivities of the C_2H_6/C_2H_4 (1 : 1, v/v) mixture for **7b** with previously reported pure organic C_2H_6-selective adsorbents at 298 K and 1 bar. (f) The experimental breakthrough curve of **7b** for C_2H_6/C_2H_4 (1/1, v/v, no carrier gas) at 298 K and 1 bar with a total flow rate was 5 mL min^{-1}.

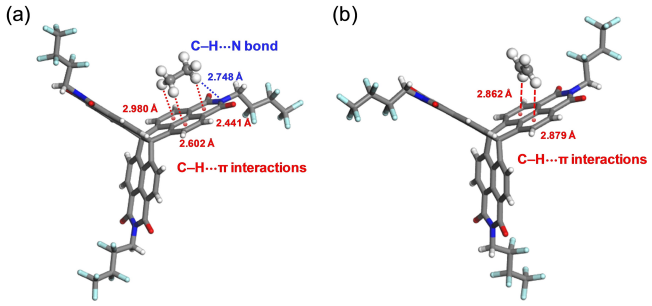

Figure 5. The calculated C–H···π interactions, C–H···N bond, and adsorption sites in **7b** for C_2H_6 (a) and C_2H_4 (b).

a single step,[23] which offers the appealing opportunity for industrial applications.

In order to further assess the gas separation effect of **7b**, the dynamic breakthrough experiment of C_2H_6/C_2H_4 mixed gas (1/1, v/v, total inlet flow rate was 5 mL min^{-1}) was carried out. Figure 4f shows that **7b** has good separation performance towards C_2H_6, and the breakthrough time of **7b** is about 140 s, with the separation factor of 2.13, consistent with the value of 2.24 calculated by IAST. The separation performance of **7b** can be maintained even after 5 cycles in the dynamic C_2H_6/C_2H_4 column breakthrough test under the same conditions (Figure S7), demonstrating its good regeneration and reusability. Additionally, **7b** shows extremely high chemical stability (Figure S11). Together, these data showcase the potential value of propellane system with a unique conformational space for gas separation.[24]

In conclusion, we have reported the synthesis of a new kind of propellane, featuring the fusion of NMI units to [3.3.3] propellane. The resulting molecular structure is unambiguously confirmed by X-ray crystallography, which reveals a quasi-D_{3h} symmetry. Due to the strong homoconjugation between the NMI subunits, the propellane triimide shows large bathochromic shift, amplified molar absorptivity, enhanced fluorescence, and lower reduction potential when compared to NMI subunit. The fluoroalkyl substituents at the imide positions promote the solid-state packing into porous 3D superstructure, which has demonstrated the high potential application in C_2H_6/C_2H_4 separation. It should be noted that, from a synthetic point of view, the propellane triimide will be uniquely valuable scaffold, enabling access to a variety of complex propellane systems that display strong homoconjugation, high fluorescence, and capability for efficient separation and organic optoelectronic devices.

Acknowledgements

We thank the financial support of National Key Research and Development Program of China (2022YFC2106100) and the National Natural Science Foundation of China (NSFC) (21871022, 22175013, 22275011).

Conflict of Interest

The authors declare no conflict of interest.

Data Availability Statement

The data that support the findings of this study are available in the supplementary material of this article.

Keywords: propellane triimide · three-dimensional · homoconjugation · crystal packing · gas separation

[1] a) T. M. Swager, *Acc. Chem. Res.* **2008**, *41*, 1181; b) J. H. Chong, M. J. MacLachlan, *Chem. Soc. Rev.* **2009**, *38*, 3301; c) C.-F. Chen, *Chem. Commun.* **2011**, *47*, 1674; d) D. Kuck, *Chem. Rev.* **2006**, *106*, 4885; e) D. Kuck, *Chem. Rec.* **2015**, *15*, 1075.

[2] a) Y. Han, Z. Meng, Y.-X. Ma, C.-F. Chen, *Acc. Chem. Res.* **2014**, *47*, 2026; b) J. R. Weidman, R. Guo, *Ind. Eng. Chem. Res.* **2017**, *56*, 4220; c) N. T. Tsui, A. J. Paraskos, L. Torun, T. M. Swager, E. L. Thomas, *Macromolecules* **2006**, *39*, 3350; d) T. M. Long, T. M. Swager, *J. Am. Chem. Soc.* **2002**, *124*, 3826; e) H. Ma, J. Chen, L. Tan, J. Bu, Y. Zhu, B. Tan, C. Zhang, *ACS Macro Lett.* **2016**, *5*, 1039.

[3] a) E. H. Menke, V. Lami, Y. Vaynzof, M. Mastalerz, *Chem. Commun.* **2016**, *52*, 1048; b) P. Biegger, S. Stolz, S. N. Intorp, Y. Zhang, J. U. Engelhart, F. Rominger, K. I. Hardcastle, U. Lemmer, X. Qian, M. Hamburger, U. H. F. Bunz, *J. Org. Chem.* **2015**, *80*, 582; c) K. Kawasumi, T. Wu, T. Zhu, H. S. Chae, T. V. Voorhis, M. A. Baldo, T. M. Swager, *J. Am. Chem. Soc.* **2015**, *137*, 11908; d) N. Seiki, Y. Shoji, T. Kajitani, F. Ishiwari, A. Kosaka, T. Hikima, M. Takata, T. Someya, T. Fukushima, *Science* **2015**, *348*, 1122; e) T. Yokota, T. Kajitani, R. Shidachi, T. Tokuhara, M. Kaltenbrunner, Y. Shoji, F. Ishiwari, T. Sekitani, T. Fukushima, T. Someya, *Nat. Nanotechnol.* **2018**, *13*, 139; f) S. R. Peurifoy, E. Castro, F. Liu, X. Zhu, F. Ng, S. Jockusch, M. L. Steigerwald, L. Echegoyen, C. Nuckolls, T. J. Sisto, *J. Am. Chem. Soc.* **2018**, *140*, 9341.

[4] a) Y. Jiang, C.-F. Chen, *Eur. J. Org. Chem.* **2011**, 6377; b) Y.-X. Ma, Z. Meng, C.-F. Chen, *Synlett* **2015**, *26*, 6, and references therein.

[5] a) B. Kohl, F. Rominger, M. Mastalerz, *Org. Lett.* **2014**, *16*, 704; b) D. Reinhard, F. Rominger, M. Mastalerz, *J. Org. Chem.* **2015**, *80*, 9342; c) S. Langis-Barsetti, T. Maris, J. D. Wuest, *J. Org. Chem.* **2018**, *83*, 15426; d) B. Kohl, F. Rominger, M. Mastalerz, *Chem. Eur. J.* **2015**, *21*, 17308; e) B. Kohl, F. Rominger, M. Mastalerz, *Angew. Chem. Int. Ed.* **2015**, *54*, 6051; f) K. Baumgärtner, A. L. M. Chincha, A. Dreuw, F. Rominger, M. Mastalerz, *Angew. Chem. Int. Ed.* **2016**, *55*, 15594; g) B. Kohl, M. V. Bohnwagner, F. Rominger, H. Wadepohl, A. Dreuw, M. Mastalerz, *Chem. Eur. J.* **2016**, *22*, 646.

[6] a) Y. Duan, G. Zhang, X. Liu, F. Shi, T. Wang, H. Yan, H. Xu, L. Zhang, *J. Org. Chem.* **2022**, *87*, 8841; b) K. Baumgärtner, M. Hoffmann, F. Rominger, S. M. Elbert, A. Dreuw, M. Mastalerz, *J. Org. Chem.* **2020**, *85*, 15256; c) L. Ueberricke, B. P. Benke, T. Kirschbaum, S. Hahn, F. Rominger, U. H. F. Bunz, M. Mastalerz, *Chem. Eur. J.* **2021**, *27*, 2043; d) M. R. Talipov, T. S. Navale, R. Rathore, *Angew. Chem. Int. Ed.* **2015**, *54*, 14468; e) J.-R. Mistry, S. Montanaro, I. A. Wright, *Mater Adv* **2023**, *4*, 787; f) S. Montanaro, D. G. Congrave, M. K. Etherington, I. A. Wright, *J. Mater. Chem. C* **2019**, *7*, 12886; g) S. Montanaro, P. Pander, J.-R. Mistry, M. R. J. Elsegood, S. J.

Teat, A. D. Bond, I. A. Wright, D. G. Congrave, M. K. Etherington, *J. Mater. Chem. C* **2022**, *10*, 6306.
[7] a) G. Dyker, J. Körning, P. G. Jones, P. Bubenitschek, *Angew. Chem. Int. Ed.* **1993**, *32*, 1733; b) G. Dyker, T. Kerl, J. Körning, P. Bubenitschek, P. G. Jones, *Tetrahedron.* **2000**, *56*, 8665; c) T. Kubo, S. Miyazaki, T. Kodama, M. Aoba, Y. Hirao, H. Kuratab, *Chem. Commun.* **2015**, *51*, 3801; d) T. Kodama, S. Miyazaki, T. Kubo, *ChemPlusChem* **2019**, *84*, 599; e) K. Kato, S. Tanaka, N. Seto, K. Wada, M. Gon, S. Fa, S. Ohtani, K. Tanaka, T. Ogoshi, *Chem. Commun.* **2023**, *59*, 7080; f) T. Kodama, Y. Hirao, T. Kubo, *Precis. Chem.* **2023**, *1*, 183.
[8] a) T. Kodama, M. Aoba, Y. Hirao, S. M. Rivero, J. Casado, T. Kubo, *Angew. Chem. Int. Ed.* **2022**, *61*, e202200688; b) T. Kodama, Y. Hirao, T. Nishiuchi, T. Kubo, *ChemPlusChem* **2017**, *82*, 1006; c) L. Lv, J. Robert, C. Xiao, Z. Jia, W. Jiang, G. Zhang, C. Risko, L. Zhang, *Chem. Sci.* **2019**, *10*, 4951; d) L. Lv, W. Sun, Z. Jia, G. Zhang, F. Wang, Z. Tan, L. Zhang, *Mater. Chem. Front.* **2020**, *4*, 3539.
[9] a) S. Seifert, K. Shoyama, D. Schmidt, F. Würthner, *Angew. Chem. Int. Ed.* **2016**, *55*, 6390; b) H. Zhylitskaya, J. Cybińska, P. Chmielewski, T. Lis, M. Stępień, *J. Am. Chem. Soc.* **2016**, *138*, 11390; c) M. Żyła-Karwowska, H. Zhylitskaya, J. Cybińska, T. Lis, P. J. Chmielewski, M. Stępień, *Angew. Chem. Int. Ed.* **2016**, *55*, 14658; d) M. Navakouski, H. Zhylitskaya, P. J. Chmielewski, T. Lis, J. Cybińska, M. Stępień, *Angew. Chem. Int. Ed.* **2019**, *58*, 4929; e) K. Shoyama, F. Würthner, *J. Am. Chem. Soc.* **2019**, *141*, 13008; f) S. A. Balahoju, Y. K. Maurya, P. J. Chmielewski, T. Lis, M. Kondratowicz, J. Cybińska, M. Stępień, *Angew. Chem. Int. Ed.* **2022**, *61*, e202200781.
[10] T. V. Pho, F. M. Toma, M. L. Chabinyc, F. Wudl, *Angew. Chem. Int. Ed.* **2013**, *52*, 1446.
[11] R. Kumar, P. J. Chmielewski, T. Lis, D. Volkmer, M. Stępień, *Angew. Chem. Int. Ed.* **2022**, *61*, e202207486.
[12] R. Shang, Y. Fu, J. Li, S. Zhang, Q. Guo, L. Liu, *J. Am. Chem. Soc.* **2009**, *131*, 5738.
[13] X. Sun, G. Shan, Y. Sun, Y. Rao, *Angew. Chem. Int. Ed.* **2013**, *52*, 4440.
[14] T. Ueda, H. Konishi, K. Manabe, *Org. Lett.* **2012**, *14*, 5370.
[15] B. W. D'Andrade, S. Datta, S. R. Forrest, P. Djurovich, E. Polikarpov, M. E. Thompson, *Org. Electron.* **2005**, *6*, 11.
[16] Deposition numbers 2297714 (for **7a**) and 2297744 (for **7b**) contain the supplementary crystallographic data for this paper. These data are provided free of charge by the joint Cambridge Crystallographic Data Centre and Fachinformationszentrum Karlsruhe Access Structures service.
[17] P. Debroy, S. V. Lindeman, R. Rathore, *Org. Lett.* **2007**, *9*, 4091.
[18] a) L. Li, H. Ma, J. Zhang, E. Zhao, J. Hao, H. Huang, H. Li, P. Li, X. Gu, B. Z. Tang, *J. Am. Chem. Soc.* **2021**, *143*, 3856; b) L. Li, S. Zhao, H. Huang, M. Dong, J. Liang, H. Li, J. Hao, E. Zhao, X. Gu, *Adv. Sci.* **2023**, 2303057.
[19] a) Z. Chang, D.-H. Yang, J. Xu, T.-L. Hu, X.-H. Bu, *Adv. Mater.* **2015**, *27*, 5432; b) M. Handke, H. Weber, M. Lange, J. Möllme, J. Lincke, R. Gläser, R. Staudt, H Krautscheid, *Inorg. Chem.* **2014**, *53*, 7599.
[20] a) A. Corma, E. Corresa, Y. Mathieu, L. Sauvanaud, S. Al-Bogami, M. S. Al-Ghramib, A. Bourane, *Catal. Sci. Technol.* **2017**, *7*, 12; b) J. Li, R. J. Kuppler, H. Zhou, *Chem. Soc. Rev.* **2009**, *38*, 1477.
[21] X. Zhang, J. Wang, L. Li, J. Pei, R. Krishna, H. Wu, W. Zhou, G. Qian, B. Chen, B. Li, *Angew. Chem. Int. Ed.* **2021**, *60*, 10304.
[22] a) F. Jin, E. Lin, T. Wang, S. Geng, T. Wang, W. Liu, F. Xiong, Z. Wang, Y. Chen, P. Cheng, Z. Zhang, *J. Am. Chem. Soc.* **2022**, *144*, 5643; b) C. He, Y. Wang, Y. Chen, X. Wang, J. Yang, L. Li, J. Li, *ACS Appl. Mater. Interfaces* **2020**, *12*, 52819; c) J. Wang, X. Lian, Z. Zhang, X. Liu, Q. Zhao, J. Xu, X. Cao, B. Li, X. Bu, *Chem. Commun.* **2023**, *59*, 11240; d) L. A. Baldwin, J. W. Crowe, D. A. Pyles, P. L. McGrier, *J. Am. Chem. Soc.* **2016**, *138*, 15134; e) T. Yoon, S. B. Baek, D. Kim, E. Kim, W. Lee, B. K. Singh, M. S. Lah, Y. Bae, K. S. Kim, *Chem. Commun.* **2018**, *54*, 9360; f) Y. Chang, H. Huang, H. Zhu, Y. Zhao, L. Wang, Y. Sun, C. Zhong, *Chem. Eng. J.* **2020**, *427*, 131726; g) X. Zhang, L. Li, J. Wang, H. Wen, R. Krishna, H. Wu, W. Zhou, Z. Chen, B. Li, G. Qian, B. Chen, *J. Am. Chem. Soc.* **2020**, *142*, 633.
[23] a) K. Su, W. Wang, S. Du, C. Ji, D. Yuan, *Nat. Commun.* **2021**, *12*, 3703; b) R. Lin, L. Li, H. Zhou, H. Wu, C. He, S. Li, R. Krishna, J. Li, W. Zhou, B. Chen, *Nat. Mater.* **2018**, *17*, 1128.
[24] a) R. G. D. Taylor, C. G. Bezzu, M. Carta, K. J. Msayib, J. Walker, R. Short, B. M. Kariuki, N. B. McKeown, *Chem. Eur. J.* **2016**, *22*, 2466; b) K. Kato, N. Seto, K. Chida, T. Yoshii, M. Mizuno, H. Nishihara, S. Ohtani, T. Ogoshi, *Bull. Chem. Soc. Jpn.* **2022**, *95*, 1296; c) K. Kato, T. Hiroi, N. Seto, S. Ohtani, T. Ogoshi, *Chem. Lett.* **2022**, *51*, 975.

Manuscript received: January 24, 2024
Accepted manuscript online: February 28, 2024
Version of record online: March 14, 2024